Compressible boundary layer transition induced by isolated roughness elements

By M. Bernardini†, S. Pirozzoli†, P. Orlandi† AND S. K. Lele‡

The laminar-to-turbulent transition of boundary layers induced by isolated three-dimensional roughness elements is analyzed by mining a direct numerical simulation database, which covers the variation of many physical parameters, including Mach and Reynolds numbers, and obstacle shape and size. We find that the transition process is approximately controlled by a Reynolds number based on the momentum deficit past the obstacle, which is proportional to the classical roughness Reynolds number, and that approximately incorporates the effects of the roughness element shape. The analysis of the perturbation energy past the obstacle shows that the varicose mode of instability is always dominant in the close proximity of the obstacle, and it promotes transition in super-critical flow cases. On the other hand, the sinuous mode appears to dominate the evolution of marginally sub-critical cases, which feature quasi-steady momentum streaks.

1. Introduction

The laminar-to-turbulent transition of boundary layers induced by three-dimensional roughness elements is important for aerospace applications because of its impact on the prediction and control of skin friction and heat transfer, especially in high-speed applications involving transonic and supersonic (external and internal) flows. For instance, the accurate prediction of transition is crucial for the design of the thermal protection systems of hypersonic vehicles. Despite the substantial number of studies of both experimental and numerical nature on this topic, the mechanisms leading to transition are still poorly understood, and this is particularly true in the supersonic and hypersonic regime, in which it is difficult to make accurate measurements (Schneider 2001).

The typical effect of a three-dimensional roughness element on a laminar boundary layer is to abruptly shift the transition location upstream with respect to the case of natural transition (i.e., for a smooth surface), with the amount of movement increasing with the roughness height (k). Early experiments (Dryden 1953) suggested that transition is determined by the flow properties at the edge of the roughness element (hereinafter denoted with the subscript k) through a roughness Reynolds number

$$Re_k = \rho_k \, u_k \, k/\mu_k. \tag{1.1}$$

However, this parameter cannot account for several effects, including roughness shape and wall temperature. Currently, the prediction of roughness-induced transition at high-speed heavily relies on empirical correlations, a popular one being the Re_θ/M_∞ criterion (Reshotko 2007).

Past efforts have identified the typical paths to transition, especially in the low-speed regime. Experiments have shown that the flow around an isolated three-dimensional roughness element is characterized by the presence of a steady horseshoe vortex that

† Dipartimento di Ingegneria Meccanica e Aerospaziale, Università di Roma 'La Sapienza'
‡ Department of Aeronautics and Astronautics, Stanford University

wraps around the obstacle, with two steady counter-rotating vortices trailing downstream. The streamwise vortices and the associated low-momentum streak lead to a convective shear-layer instability in the wake of the roughness element, characterized by periodic shedding of hairpin-like vortical structures (Acarlar & Smith 1986; Klebanoff *et al.* 1992). According to Ergin & White (2006), transition occurs when the growth of fluctuations is sufficient to trigger transition and to penetrate the wall layer. These observations are in agreement with transient growth theory, predicting that optimal perturbations are associated with steady streamwise vortices (Tumin & Reshotko 2003).

Recent direct numerical simulations (DNS) (Groskopf *et al.* 2008; Marxen *et al.* 2010; Redford *et al.* 2010; Choudhari *et al.* 2010; Bernardini *et al.* 2012) performed in the supersonic and hypersonic regime indicate that the same scenario observed at low speed also holds at higher Mach numbers, with minor changes caused by compressibility. The numerical studies have highlighted the importance of the unstable detached shear layer forming on the top of the roughness element and have identified the wake behind the roughness element as the primary source for transition.

The aim of this work is to perform a numerical study of the laminar-to-turbulent transition of compressible zero-pressure-gradient boundary layers over a flat plate induced by the presence of isolated three-dimensional roughness elements. An effort has been made to widen the range of flow conditions analyzed in previous studies to cover the variation of many physical parameters, including Mach and Reynolds numbers, wall temperature conditions, as well as the obstacle shape and size. The main objective is to understand their influence on the transition mechanisms in the obstacle wake and to identify a (possibly) universal parameter controlling roughness-induced transition.

2. Numerical strategy and DNS database

The Navier-Stokes equations are discretized on a Cartesian mesh and solved by means of a conservative finite-difference approach. The flow solver relies on sixth-order central discretization of the convective terms of the Navier-Stokes equations cast in split form (Pirozzoli 2010), and it allows capture of shock waves by means of localized application of fifth-order WENO numerical reconstructions controlled by the Ducros shock sensor (Pirozzoli *et al.* 2010). The diffusive terms are expanded to Laplacian form for improved stability and also approximated with sixth-order central difference formulas. The resulting semi-discrete ODE system is advanced in time through an explicit low-storage third-order Runge-Kutta algorithm (Bernardini & Pirozzoli 2009). The numerical method used is particularly suitable for the simulation of transitional flows, because it is based on the concept of preservation of the total kinetic energy at the discrete level (in the limit of inviscid incompressible flow and vanishing integration time step), thus yielding stable numerical solutions without needing extra numerical dissipation. The roughness element is handled through an extension of the immersed boundary method (Pirozzoli *et al.* 2012), which allows simple and effective coupling with the flow solver.

The computational domain is a Cartesian box, extending for $L_x = 70\,\delta$, $L_y = 20\,\delta$, $L_z = 6\,\delta$ in the streamwise (x), wall-normal (y) and spanwise (z) directions, where δ, the boundary layer thickness at the inflow station, is chosen as reference length. The domain is discretized with a grid consisting of $N_x = 2048$, $N_y = 171\,N_z = 256$ points, clustered close to the wall according to a hyperbolic sine mapping function. A non-uniform distribution in the streamwise and spanwise direction was also used to allow better resolution in the region close to the obstacle, and the roughness element is resolved

with at least twenty grid points in each direction. The grid size has been selected after a grid sensitivity study, which is not reported here due to space limitations.

The roughness element, centered at $x_c = 15\delta$, perturbs the laminar boundary layer. The initial condition is determined from compressible similarity solution and is also used to prescribe the inflow. Radiative boundary conditions are assigned at the top and outflow boundaries, and periodicity is enforced in the spanwise direction, implying that the actual simulated flow is that around a periodic array of identical roughness elements.

A critical issue in transitional flows is the characterization of the external disturbance environment (van Driest & Blumer 1962), especially in the supersonic regime, where the boundary layer is quite receptive to free-stream disturbances. This issue was discussed by Redford *et al.* (2010), who stimulated the flow with acoustic disturbances. In our simulations, perturbations are triggered within the incoming boundary layer in the form of random fluctuations of all three velocity components, with maximum amplitude of 0.5% of the free-stream velocity. A preliminary analysis performed for representative high-Mach number cases has shown that this level of disturbances does promote flow breakdown in the absence of the roughness element.

Roughness-induced transition in the compressible regime is controlled by many parameters. In our numerical database we tried to cover a large portion of the available parameter space, considering variations of: (*a*) Mach number (from $M_\infty = 1.1$ to $M_\infty = 6$); (*b*) Reynolds number of the incoming boundary layer (the available range in terms of roughness Reynolds number (as defined in equation (1.1)) is $Re_k = 400-1300$); (*c*) obstacle height as a fraction of the boundary layer thickness ($k/\delta = 0.15, 0.2, 0.25, 0.3, 0.4, 0.7$); (*d*) wall temperature conditions ($1 \leq T_w/T_{aw} \leq 2$, where T_w and T_{aw} are the wall and the adiabatic wall temperature, respectively) and (*e*) roughness shapes (hemispheres, cubes and cylinders). Moreover, for the cylindrical elements we also performed simulations, changing the obstacle aspect ratio, i.e., the ratio of height to diameter ($k/D = 0.5, 1, 2$). A limited set of results is shown in the following. The analysis of the full database will be the subject of future publications.

3. Overview of the transition process

To highlight the qualitative features of the transition process at the various flow conditions, we focus here on the hemispherical roughness element, under adiabatic wall conditions. The time-averaged skin friction coefficient in the symmetry plane is shown in Figure 1. At all Mach numbers, two flow states occur, depending on the Reynolds number. In the sub-critical state, the boundary layer remains laminar, and the skin friction decreases steadily past the obstacle all the way to the end of the computational domain. In the super-critical state, the amplitude of the disturbance caused by the roughness element is sufficient to promote flow breakdown, as indicated by the rapid rise of the skin friction coefficient. For a given Mach number, the transition point moves upstream as the Reynolds number is increased, attaining a limiting value for which the roughness is said to be effective, and further increase of the Reynolds number does not lead to movement of the transition point. A clear interesting effect of compressibility is observed on such a limited position, which increases with the Mach number.

Similar considerations can also be drawn looking at the typical structures characterizing the roughness-induced transition process, shown in Figure 2 through isosurfaces of the swirling strength (i.e., the imaginary part of the intermediate eigenvalue of the velocity gradient tensor) for representative super-critical flow cases. Regardless of the

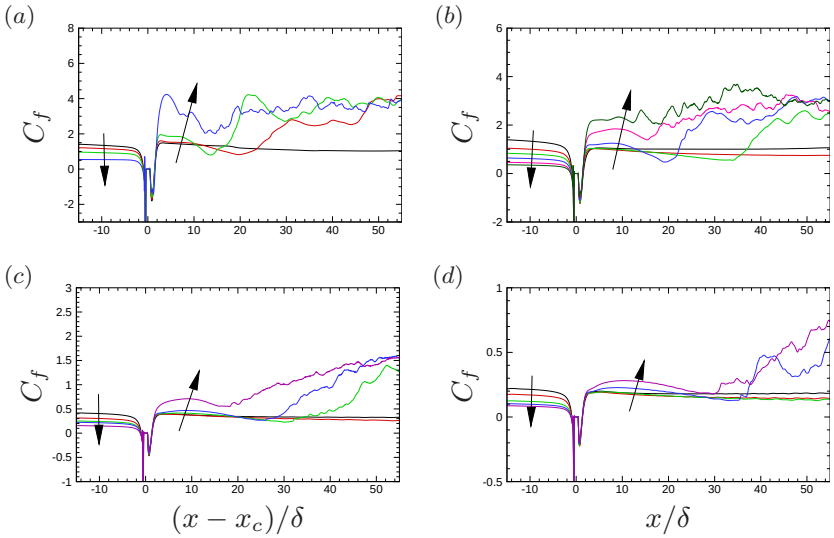

FIGURE 1. Mean skin friction coefficient along the symmetry line for hemispherical roughness element with size $k/\delta = 0.4$. (a), $M_\infty = 1.1$, $Re_\delta = 2500, 2900, 3655, 6500$; (b), $M_\infty = 2$, $Re_\delta = 3000, 4000, 5000, 65000, 9000, 11500$; (c), $M_\infty = 4$, $Re_\delta = 15000, 20000, 25000, 28000, 40000$; and (d), $M_\infty = 6$, $Re_\delta = 40000, 50000, 70000, 85000, 100000$. The arrows indicate the direction of increasing Re_δ.

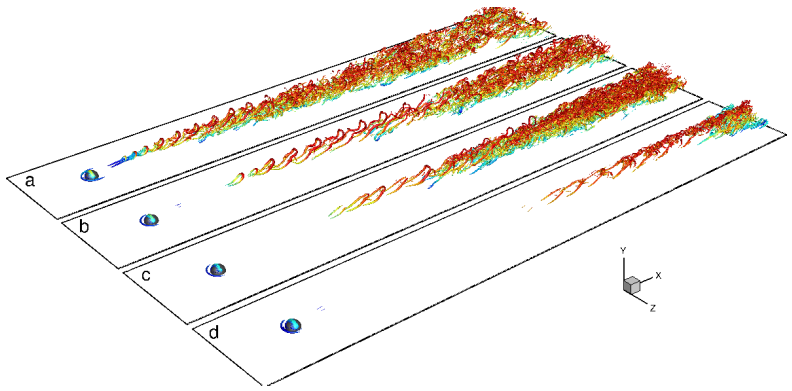

FIGURE 2. Coherent vortical structures for flow around hemispherical roughness element. (a), $M_\infty = 1.1$, $Re_\delta = 6500$; (b), $M_\infty = 2$, $Re_\delta = 9000$; (c), $M_\infty = 4$, $Re_\delta = 40000$; and (d), $M_\infty = 6$, $Re_\delta = 85000$. Vortices are educed as isosurfaces of swirling strength, and colored with the streamwise velocity.

Mach number, the most prominent feature is the shedding of hairpin vortices past the roughness element, which propagate downstream leading to flow breakdown. The generation and the evolution mechanisms of these structures have been widely discussed in the low-speed regime by Acarlar & Smith (1986) and Klebanoff *et al.* (1992), and they are mainly related to the instability characteristics of the shear layer behind the obstacle. As for the skin friction, the main effect of the compressibility is to delay the flow breakdown, and the hairpin structures look more elongated as M_∞ increases.

To further characterize the influence of compressibility on the transition process, we look at the frequency of hairpin shedding past the roughness element. For this purpose,

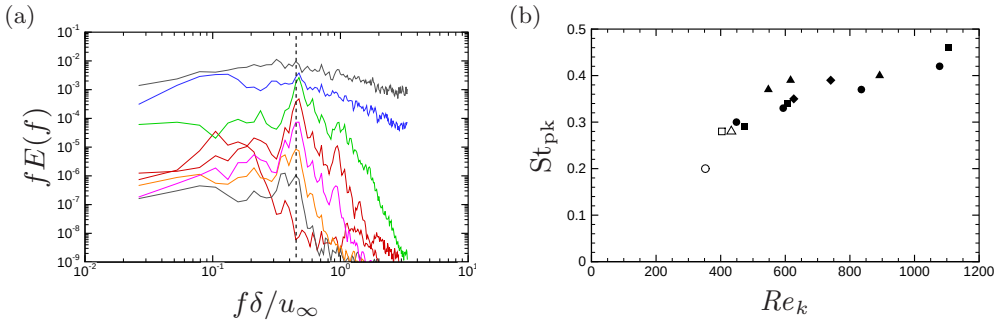

FIGURE 3. Pre-multiplied frequency spectra of the streamwise velocity are shown in frame (a) at several streamwise stations ($x/\delta = 5, 17, 18, 19, 20, 23, 30, 40$, from bottom to top) in the symmetry plane at $y = k$, for hemisphere at $M_\infty = 4$, $Re_\delta = 40000$. The vertical dashed line marks the peak frequency (f_{pk}). Frame (b) shows the peak Strouhal number ($\mathrm{St_{pk}} = f_{\mathrm{pk}}\, k/u_k$) derived from maps as in frame (a), for flow behind hemispherical obstacles, as a function of Re_k. Symbols: squares, $M_\infty = 1.1$; circles, $M_\infty = 2$; triangles, $M_\infty = 4$; diamonds, $M_\infty = 6$. Solid and hollow symbols correspond to super-critical and sub-critical cases, respectively.

the time-resolved streamwise velocity signal was stored along the centerline of the computational domain at an off-wall location corresponding to the edge of the roughness element ($y = k$). Pre-multiplied frequency spectra taken at different streamwise locations are shown in Figure 3(a) for a super-critical flow case. As expected, the spectral densities immediately past the obstacle are characterized by a distinct peak, which is the signature of quasi-periodic shedding. The peak slowly vanishes at downstream stations, where the flow breakdowns, approaching a fully turbulent state, as indicated by the more broad-banded spectra. The typical Strouhal number ($\mathrm{St_{pk}} = f_{\mathrm{pk}}\, k/u_k$) associated with the vortex shedding is shown in Figure 3(b) as a function of the roughness Reynolds number, for the hemisperical roughness element. Consistent with previous low-speed studies (Acarlar & Smith 1986; Klebanoff *et al.* 1992), the Strouhal is found to increase with Re_k, in the present case ranging from $\mathrm{St_{pk}} = 0.2$ to $\mathrm{St_{pk}} = 0.4$. Apparently, the effect of Mach number is not significant when the roughness height and edge velocity u_k are used to form the Strouhal number.

4. Characterization of the roughness element wake

The evolution of the velocity disturbances past the roughness element is characterized with focus on possible changes (if any) caused by flow compressibility. We follow Ergin & White (2006) and track the total disturbance energy associated with the unsteady velocity fluctuations,

$$e(x) = \iint \left[u'_{\mathrm{rms}}(x, y, z)\right]^2 \mathrm{d}y\mathrm{d}z, \tag{4.1}$$

where $u'_{\mathrm{rms}}(x, y, z)$ is the root-mean-square (rms) streamwise velocity. We also consider the symmetric and antisymmetric parts of the disturbance energy $e(x)$ with respect to the symmetry plane, indicated as $e_e(x)$ (even), and $e_o(x)$ (odd), respectively.

In Figure 4 we show the perturbation energy for representative hemisphere flow cases. The total perturbation energy is shown by the solid curves, whereas the perturbation energy associated with symmetric disturbances with respect to the symmetry plane (varicose mode) is shown by the dashed curves, and the energy of anti-symmetric disturbances (sinuous mode) is shown by the dot-dashed curves. For all flow cases corresponding to

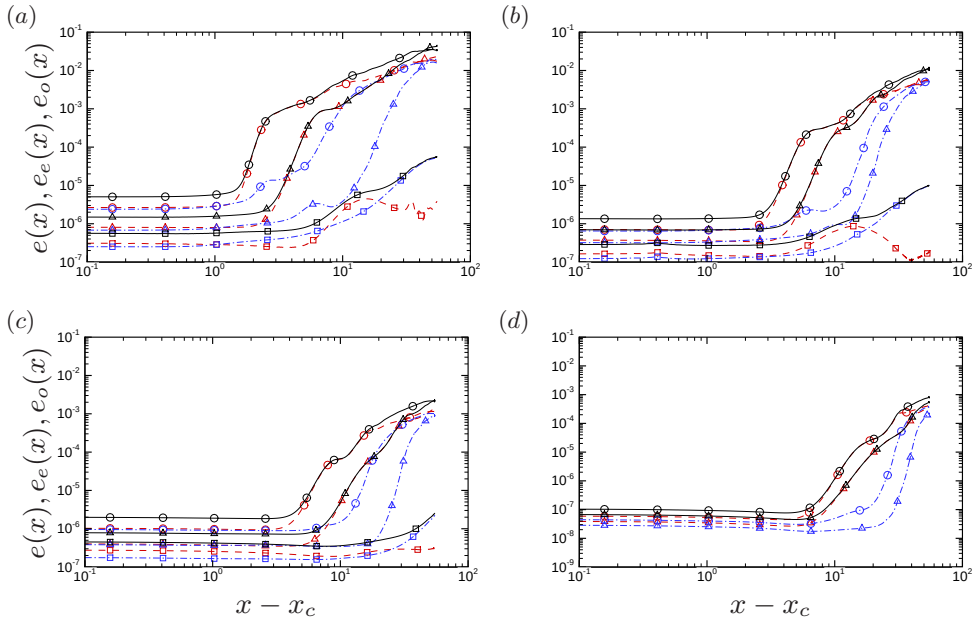

FIGURE 4. Integrated perturbation energy past hemispherical obstacles with $k/\delta = 0.4$. Solid lines: total perturbation energy (e); dashed lines: symmetric part (e_e); dot-dashed lines: anti-symmetric part (e_o). (a), $M_\infty = 1.1$, $Re_\delta = 2500$ (*squares*), 3655 (*triangles*), 6500 (*circles*); (b), $M_\infty = 2$, $Re_\delta = 4000$ (*squares*), 5000 (*triangles*), 9000 (*circles*); (c), $M_\infty = 4$, $Re_\delta = 20000$ (*squares*), 28000 (*triangles*), 40000 (*circles*); (d), $M_\infty = 6$, $Re_\delta = 85000$ (*squares*), 10000 (*circles*).

super-critical conditions the disturbance energy follows an exponential growth in a region downstream of the roughness element, which occurs over a few boundary layer thicknesses. This stage is followed by a saturation zone (which extends over O(10) boundary layer thicknesses) with a slower exponential growth, followed by a turbulent-like state. While this behavior is apparent at $M_\infty = 1.1$ and $M_\infty = 2$, the growth of the energy norm is more gradual as the Mach number increases, and, in agreement with the observations of the previous section, the higher is the Mach number, the farther is the breakdown point. It is noteworthy that for all super-critical cases, regardless of the Mach number, virtually all the energy is concentrated into the symmetric mode of perturbation, whereas the anti-symmetric mode has negligible energy, and it picks up only after saturation is complete, the two modes attaining similar magnitude in the turbulent region. This behavior can be interpreted as a confirmation that across the Mach number range here investigated, the primary mechanism for transition is related to the streamwise velocity deficit behind the roughness element, characterized by a strong detached shear layer ($\partial U/\partial y$), rather than to the side shear layers ($\partial U/\partial z$). In the sub-critical cases, the perturbation energy is still amplified by about two orders of magnitude compared with that of its upstream value, but it tends to quickly level off, and transition does not take place. In this case, the symmetric mode is still dominant during the initial amplification stage, but it gets damped after saturation is complete and the energy becomes concentrated in the antisymmetric mode. Again, this behavior seems to apply to all the Mach numbers here explored.

5. Parametrization of the by-pass transition process

Our goal here is to identify a (possibly) general threshold parameter for the onset of by-pass transition induced by the roughness element. Many generalizations of the roughness Reynolds number criterion to the compressible case have been proposed (van Driest & Blumer 1962; Redford *et al.* 2010; Bernardini *et al.* 2012). Based on the analysis of the present database, we find that a convenient generalization of Re_k is

$$Re_{kw} = \frac{\rho_k u_k k}{\mu_w}, \tag{5.1}$$

where the density is evaluated at the obstacle edge, and the dynamic viscosity is taken at the wall. Note that Eq. (5.1) quantifies the ratio between the inertia forces at the edge of the obstacle and the viscous stress at the wall. The performance of Re_{kw} as a controlling by-pass transition parameter can be judged looking at the maps shown in Figure 5 (left column), in which hollow symbols correspond to sub-critical flow cases and solid symbols correspond to super-critical cases. As stated in Sect. 3, to detect transition onset we monitor the evolution of the time-averaged skin friction coefficient past the obstacle. While no doubts exist for super-critical cases, the stipulation of a flow as sub-critical is the subject of some uncertainty, owing to the finite streamwise extent of the computational domain. The figure must thus be interpreted with some caution in the sub-critical region. As evident in Figure 5, the sub-critical and super-critical conditions are well segregated by Re_{kw}, which is promising in taking into account the effect of variations in the Mach and Reynolds number, roughness height and wall temperature. Such segregation would not be recovered using the conventional definition of roughness Reynolds number given in Eq. (1.1). However, the critical value of Re_{kw} is not the same for all the roughness elements, and it ranges from 400 to 700.

To overcome the limitations of Re_{kw} criterion we propose an alternative controlling parameter, based on the observation that the main effect of the presence of the obstacle is a deficit in the mass flux (i.e., in the streamwise momentum) downstream of it, which translates into the formation of a low-momentum streak and of a pair of counter-rotating vortices. We then consider a Reynolds number formed with the momentum defect (Q, to be estimated), the maximum cross-stream section of the obstacle and the wall viscosity,

$$Re_Q = \frac{Q S_{yz}^{1/2}}{\mu_w}, \tag{5.2}$$

where $S_{yz} \sim k \cdot D$. It is possible to provide a rough estimate for Q by assuming that the upstream boundary layer is not affected by the obstacle, and estimate the mass flux deficit due to the presence of the roughness element. Assuming that the incoming velocity profile is linear up to the edge of the obstacle, it is easy to obtain the following estimate

$$Q \approx \rho_k \, k \, D \, u_k \, F(\text{shape}), \tag{5.3}$$

where

$$F(\text{shape}) = \int_0^1 \eta \, w^*(\eta) \mathrm{d}\eta, \tag{5.4}$$

with $\eta = y/k$, and $w^*(\eta) = w(y)/D$ defines the cross-sectional shape of the obstacle. It is then easy to relate Re_Q to Re_{kw} through

$$Re_Q = Re_{kw} \cdot (D/k)^{1/2} \cdot F(\text{shape}), \tag{5.5}$$

showing promise of Re_Q to incorporate the effects of the obstacle shape and aspect ratio.

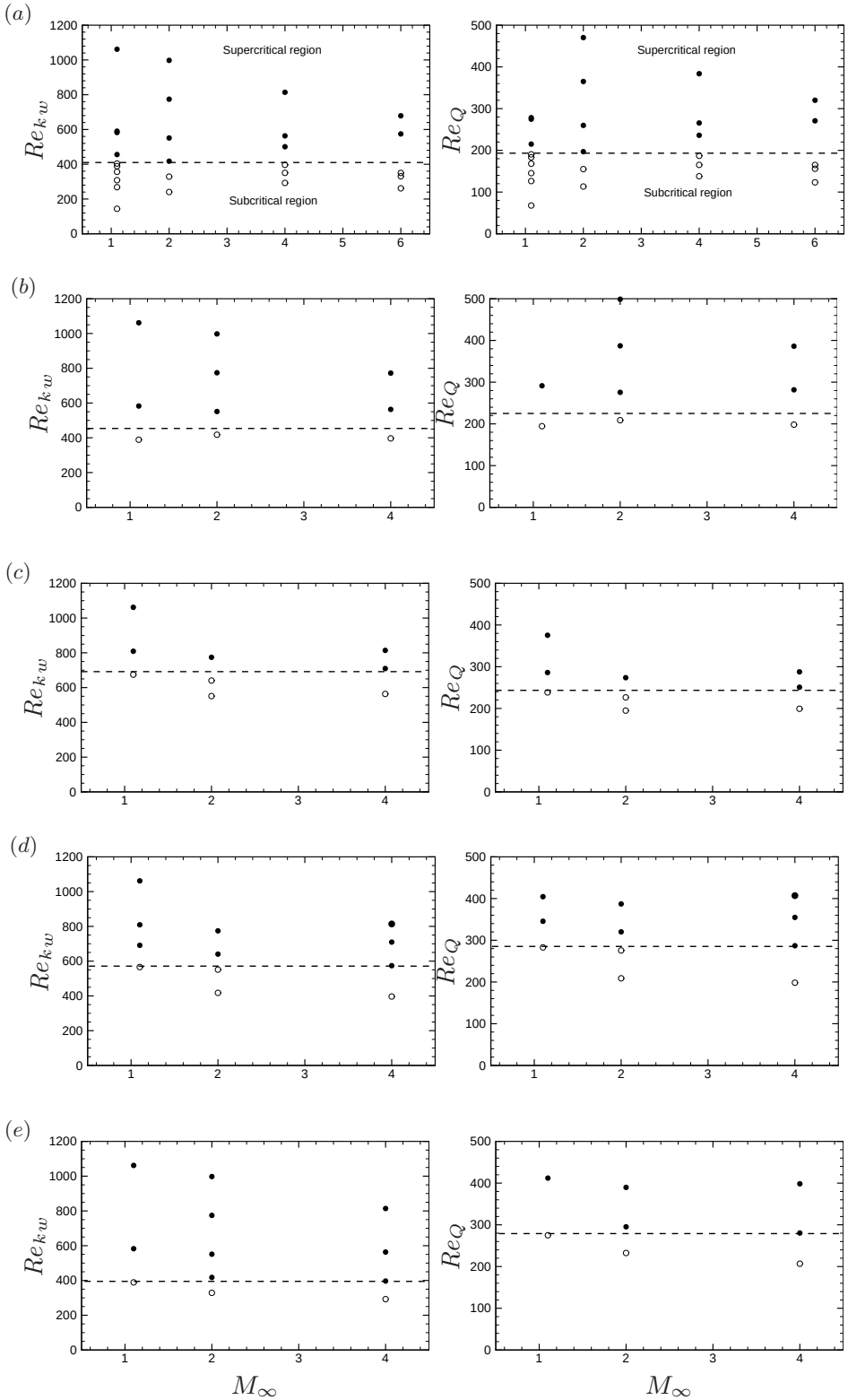

FIGURE 5. Transition map as a function of Re_{k_w} (left column) and Re_Q (right column). (*a*) hemispheres; (*b*) cubes; (*c*) cylinders ($D/k = 1/2$); (*d*) cylinders ($D/k = 1$); (*e*) cylinders ($D/k = 2$). Solid/open circles denote super/sub critical cases.

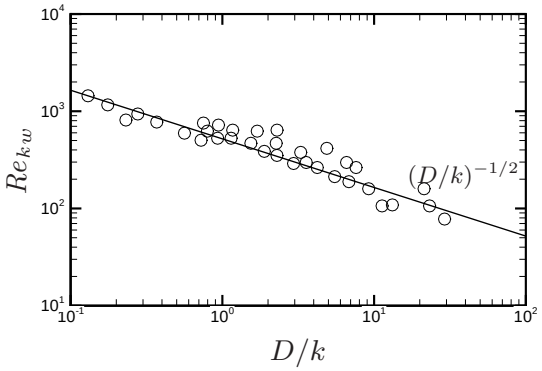

FIGURE 6. Dependence of critical roughness Reynolds number on obstacle aspect ratio (*solid line*, Eq. (5.5); symbols, experimental data (Schneider 2008))

The effectiveness of Re_Q as a by-pass transition parameter can be appreciated from Figure 5 (right column). It appears that, regardless of the object shape and/or aspect ratio, by-pass transition occurs if $Re_Q > 200 \div 280$ and if the scatter is much less than with Re_{k_w}.

Apparently, the by-pass transition criterion based on Re_Q correctly captures the experimentally observed trend with the obstacle aspect ratio. In Figure 6 we show with symbols the critical roughness Reynolds number resulting from a series of experiments (van Driest & Blumer 1962) with cylindrical obstacles of different aspect ratio. On the same graph, we show the trend of the critical roughness Reynolds number obtained from Eq. (5.5), which predicts $Re_{k_w} \sim (D/k)^{-1/2}$. Apparently, the trend is correct, and it is at least equally plausible as the frequently quoted empirical scaling $Re_{k_w} \sim (D/k)^{-2/5}$ (Schneider 2008).

6. Conclusions

We have performed a numerical study of boundary layer transition induced by isolated roughness elements, in a wide range of flow conditions. The database has allowed singling out the effects of the flow Mach and Reynolds number, of the wall temperature, and of the roughness shape and size. In all cases, the transition process is associated with the shedding of hairpin vortices past the roughness element, whose typical frequency (properly scaled) does not depend on the Mach number. The process can be parametrized with a reasonable degree of accuracy through a Reynolds number based on the estimated momentum deficit past the roughness element. Specifically, the newly designed parameter better accounts for the effect of the roughness element shape than existing correlations based on compressible extensions of the roughness Reynolds number. The evolution of the perturbation energy shows clear dominance of the varicose mode in the near field past the roughness element, which leads to transition in supercritical cases. On the other hand, under sub-critical flow conditions, the energy of the varicose mode attains a peak and then gets damped away, and the sinuous mode becomes dominant.

Acknowledgments

This research was supported by the Center for Turbulence Research, Stanford University. MB and SP also gratefully acknowledge the support of CINECA for high-performance computing resources through a 2010/2011 ISCRA grant.

REFERENCES

Acarlar, M. S. & Smith, C. R. 1986 A study of hairpin vortices in a laminar boundary layer. Part 1. Hairpin vortices generated by a hemisphere protuberance. *J. Fluid Mech.* **175**, 1–41.

Bernardini, M. & Pirozzoli, S. 2009 A general strategy for the optimization of Runge-Kutta schemes for wave propagation phenomena. *J. Comput. Phys.* **228**, 4182–4199.

Bernardini, M., Pirozzoli, S. & Orlandi, P. 2012 Compressibility effects on roughness-induced boundary layer transition. *Int. J. Heat Fluid Flow* **35**, 45–51.

Choudhari, M., Li, F., Wu, M., Chang, C., Edwards, J., Kegerise, M. & King, R. 2010 Laminart-turbulent transition behind discrete roughness elements in a high-speed boundary layer. AIAA paper 2010-1575. 40^{th} Fluid Dynamics Conference and Exhibit, Orlando, Florida.

van Driest, E. & Blumer, C. 1962 Boundary-layer transition at supersonic speeds – three-dimensional roughness effects (spheres). *J. of Aerospace Sciences* **29**, 909–916.

Dryden, H. 1953 Review of published data on the effect of roughness on transition from laminar to turbulent flow. *J. Aeronaut. Sci.* **20**, 477–482.

Ergin, F. G. & White, E. B. 2006 Unsteady and transitional flows behind roughness elements. *AIAA J.* **44**, 2504–2514.

Groskopf, G., Kloker, M. & Marxen, O. 2008 Bi-global secondary stability theory for high-speed boundary layer flows. In *Proceedings of CTR Summer program 2008*.

Klebanoff, P., Cleveland, W. & Tidstrom, K. 1992 On the evolution of a turbulent boundary layer induced by a three-dimensional roughness element. *J. Fluid Mech.* **237**, 101–187.

Marxen, O., Iaccarino, G. & Shaqfeh, E. 2010 Disturbance evolution in a Mach 4.8 boundary layer with two-dimensional roughness-induced separation and shock. *J. Fluid Mech.* **648**, 435–469.

Pirozzoli, S. 2010 Generalized conservative approximations of split convective derivative operators. *J. Comput. Phys.* **229**, 7180–7190.

Pirozzoli, S., Bernardini, M. & Grasso, F. 2010 Direct numerical simulation of transonic shock/boundary layer interaction under conditions of incipient separation. *J. Fluid Mech.* **657**, 361–393.

Pirozzoli, S., Orlandi, P. & Bernardini, M. 2012 The fluid dynamics of rolling wheels at low Reynolds number. *J. Fluid Mech.* **706**, 496–533.

Redford, J., Sandham, N. & Roberts, G. 2010 Compressibility effects on boundary-layer transition induced by an isolated roughness element. *AIAA J.* **48**, 2818–2830.

Reshotko, E. 2007 Is Re_θ/M_e a meaningful transition criterion? *AIAA J.* **44**, 1441–1443.

Schneider, S. 2001 Effects of high-speed tunnel noise on laminar-turbulent transition. *J. Spacecraft and Rockets* **38**, 323–333.

Schneider, S. 2008 Effects of roughness on hypersonic boundary-layer transition. *J. Spacecraft and Rockets* **45**, 193–209.

Tumin, A. & Reshotko, E. 2003 Optimal disturbances in compressible boundary layers. *AIAA J.* **41**, 2357–2363.